

# Dark trions govern the temperature-dependent optical absorption and emission of doped atomically thin semiconductors

Ashish Arora<sup>†,\*</sup>, Nils Kolja Wessling<sup>†</sup>, Thorsten Deilmann<sup>¶</sup>, Till Reichenauer<sup>†</sup>, Paul Steeger<sup>†</sup>, Piotr Kossacki<sup>§</sup>, Marek Potemski<sup>§,‡</sup>, Steffen Michaelis de Vasconcellos<sup>†</sup>, Michael Rohlfing<sup>¶</sup>, and Rudolf Bratschitsch<sup>†,\*</sup>

<sup>†</sup>*Institute of Physics and Center for Nanotechnology, University of Münster, Wilhelm-Klemm-Straße 10, 48149 Münster, Germany*

<sup>¶</sup>*Institute of Solid State Theory, Wilhelm-Klemm-Straße 10, University of Münster, 48149 Münster, Germany*

<sup>§</sup>*Institute of Experimental Physics, Faculty of Physics, University of Warsaw, ul. Pasteura 5, 02-093 Warszawa, Poland*

<sup>‡</sup>*Laboratoire National des Champs Magnétiques Intenses, CNRS-UGA-UPS-INS-EMFL, 25 avenue des Martyrs, 38042 Grenoble, France*

\*Email: [arora@uni-muenster.de](mailto:arora@uni-muenster.de), [Rudolf.Bratschitsch@uni-muenster.de](mailto:Rudolf.Bratschitsch@uni-muenster.de)

We perform absorption and photoluminescence spectroscopy of trions in hBN-encapsulated WSe<sub>2</sub>, WS<sub>2</sub>, MoSe<sub>2</sub>, and MoS<sub>2</sub> monolayers, depending on temperature. The different trends for W- and Mo-based materials are excellently reproduced considering a Fermi-Dirac distribution of bright and dark trions. We find a dark trion,  $X_D^-$  19 meV below the lowest bright trion,  $X_1^-$  in WSe<sub>2</sub> and WS<sub>2</sub>. In MoSe<sub>2</sub>,  $X_D^-$  lies 6 meV above  $X_1^-$ , while  $X_D^-$  and  $X_1^-$  almost coincide in MoS<sub>2</sub>. Our results agree with *GW*-BSE *ab-initio* calculations and quantitatively explain the optical response of doped monolayers with temperature.

**Introduction.** Everyday optoelectronic devices such as solar cells, photodiodes, light emitting diodes, and lasers critically depend on the knowledge about the energy level structure of the semiconducting materials. In particular, the emission of light strongly depends on optical selection rules governing the lowest-energy optical transitions. Recently, it has been found that the atomically thin semiconducting transition metal dichalcogenides (TMDCs) of the form WX<sub>2</sub> ( $X = S, Se$ ) or MoX<sub>2</sub> ( $X = S, Se, Te$ ) are fundamentally different from the optical point of view. Despite their similar crystal structure, the photoluminescence (PL) of neutral excitons in monolayer MoSe<sub>2</sub> [1–3], MoS<sub>2</sub> [3,4] and MoTe<sub>2</sub> [5] decreases from cryogenic up to room temperature, while the PL increases for monolayer WSe<sub>2</sub> [2–4,6] and WS<sub>2</sub> [3,7]. This behavior has been qualitatively explained by the presence of dark excitons. Due to the uniquely contrasting spin character of the conduction bands [1,4,6,8,9], the lowest neutral exciton transition in WX<sub>2</sub> is optically disallowed (“dark”), and it is dipole-allowed (“bright”) in MoX<sub>2</sub> [1,5,6,8–17]. Besides these spin-forbidden dark excitons, momentum-forbidden dark excitons with electron and hole residing in different valleys play a role [18,19].

The optical response of doped TMDC monolayers is governed by trions [9,20,21]. Similar to neutral excitons, bright [14,20,22] and dark [14] trions exist. However, their role in the temperature-dependent absorption and photoluminescence emission is poorly understood. In particular, dark trions are notoriously difficult to study in experiments [16,17,23]. Since doped atomically thin semiconductors hold the promise for novel ‘valleytronic’ devices [19,24], it is of utmost importance to gain a quantitative understanding of bright and dark trions.

We measure the optical absorption and PL emission of trions in TMDC monolayers of WSe<sub>2</sub>, WS<sub>2</sub>, MoSe<sub>2</sub>, and MoS<sub>2</sub> encapsulated in hBN as a function of temperature. We reveal that the combined effect of oscillator strength transfer and the thermal distribution of trions between the bright and dark states leads to the unique PL response of the different 2D semiconductors.

**Bright and dark trions.** Due to strong spin-orbit coupling, the conduction and valence bands at the K point of the Brillouin zone of TMDCs are almost completely polarized. The transitions between bands with opposite spin have vanishing oscillator strength (dark excitons/trions). Assuming a negative doping, four different types of excitations are possible: neutral bright excitons ( $X^0$ ), neutral dark excitons ( $X_D$ ), bright trions ( $X^-$ ), and dark trions ( $X_D^-$ ) [14]. Fig. S1 [25] depicts a k-space representation of these excitations and quantitative results of our *ab-initio* calculations employing the *GW*+BSE approach with its extension to trions [14,26–29]. In our calculation of WX<sub>2</sub> monolayers in vacuum,  $X_1^-$  is the lowest-bright state, while the dark trion  $X_D^-$  lies about 30 meV below  $X_1^-$ . In contrast, for MoS<sub>2</sub> and MoSe<sub>2</sub>, the dark trion  $X_D^-$  resides only 5 meV and 10 meV below the bright trion  $X_1^-$ , respectively. Because the relative accuracy of our method is about 10 meV, bright and the dark trions in Mo-based materials are almost energetically degenerate on this energy scale. The effect of surrounding hBN on the relative separation between bright and dark trions (when compared to vacuum around the monolayer) is less than 10 meV, which is within our numerical accuracy.

**Temperature-dependent absorption and emission spectra.** Figure 1(a) and 1(e) present optical absorption and PL spectra of a hBN-encapsulated WSe<sub>2</sub> monolayer, measured for temperatures  $T = 5 - 300$  K (also Fig. S3 [25]). At cryogenic temperatures, narrow resonances with nearly Lorentzian line shapes corresponding to the two trions ( $X_1^-$  and  $X_2^-$ ) and the neutral exciton  $X^0$  are clearly resolved. The presence of two trions points towards a negative doping of the WSe<sub>2</sub> monolayer [14,22,30]. Narrow linewidths (Table S1 [25]) approaching the homogeneous regime confirm the high quality of our sample [31–33].

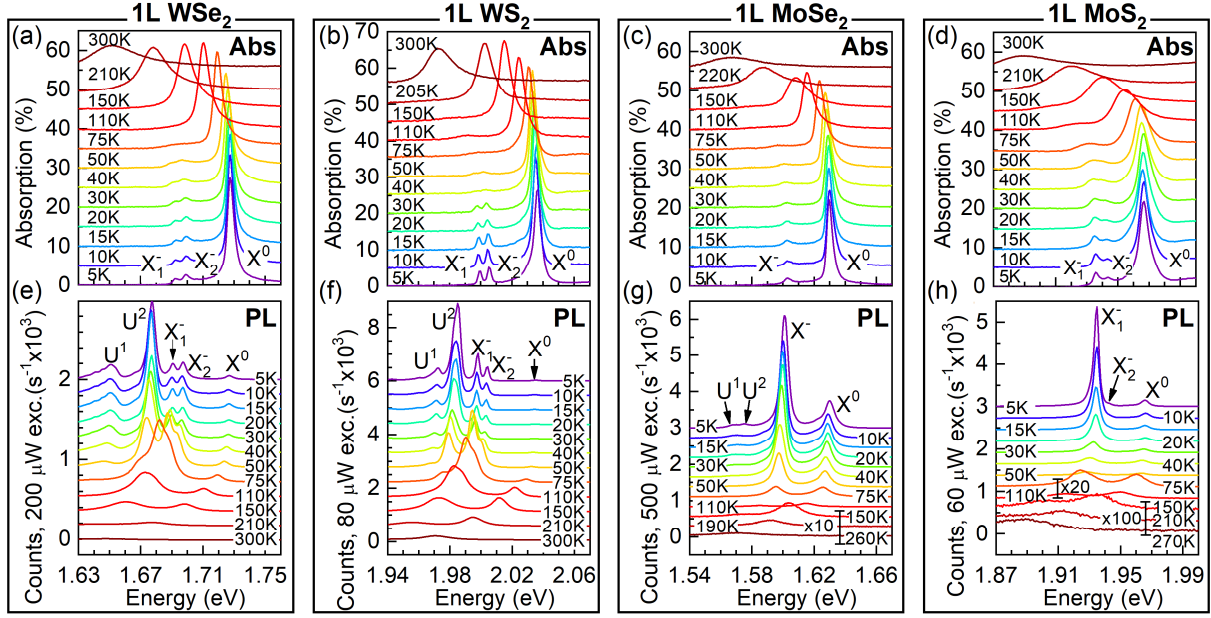


**Figure 1.** Optical absorption spectra of hBN-encapsulated (a) WSe<sub>2</sub>, (b) WS<sub>2</sub>, (c) MoSe<sub>2</sub>, and (d) MoS<sub>2</sub> monolayers on sapphire substrate, measured as a function of temperature  $T = 5 - 300$  K. (e) to (h) photoluminescence (PL) spectra as a function of temperature. The spectra are vertically shifted for clarity. Low PL intensities in (g) and (h) are amplified by factors mentioned with the spectra.

Figure 1(b) – (d) depict optical absorption and Fig. 1(f) – (h) show PL spectra at different temperatures for hBN-encapsulated 1L WS<sub>2</sub>, MoSe<sub>2</sub>, and MoS<sub>2</sub>. Similar to WSe<sub>2</sub>, WS<sub>2</sub> also exhibits two trions and one neutral exciton. The PL lines U<sup>1</sup> and U<sup>2</sup> in Fig. 1(e) and 1(f) have previously been associated either with the emission from defect-bound excitons [34] or with dark excitons coupled to chiral phonons [35]. For 1L MoS<sub>2</sub>, two trions are clearly discernible (Fig. 1(d)), in agreement with recent reports [36]. For 1L MoSe<sub>2</sub>, only one trion is visible (Fig. 1(c)). Theoretically, three nearly degenerate bright resonances are expected for MoSe<sub>2</sub>, which possibly are not resolved in the experiment [14].

**Transfer of oscillator strength between trions and excitons.** To gain a comprehensive understanding of the optical response of the 2D semiconductors at different temperatures, we fit the trion and neutral exciton resonances in the absorption and PL spectra of Fig. 1(a)-(h) with normalized Lorentzians. The area of the absorption lines is proportional to the optical oscillator strength of the transitions [37–39], which are plotted in Figs. 2(a – d). In all cases, the oscillator strength of the trions decreases as the temperature rises, while it increases for the neutral excitons (Fig. S4 [25]). This observation is in agreement with previous temperature-dependent spectroscopy of trion-exciton pairs in II-VI quantum wells [37–39], 1L WSe<sub>2</sub> [6], and 1L WS<sub>2</sub> [40], where a relationship between the excess carrier density and the trion oscillator strength was found. Such a connection has also been established in magneto-reflectance and magneto-PL spectroscopy of III-V and II-VI quantum wells [39,41,42] and TMDC monolayers [43]. The mechanism of oscillator strength transfer from trions to excitons with temperature is explained as follows.

In a doped semiconductor (considering negative doping henceforth) at thermal equilibrium, excess charges occupy phase space around the band extrema of the Brillouin zone following a Fermi-Dirac (F-D) distribution,  $F_e(T)$  (Fig. 3(a)). The thermal distribution of optically-created trions in quasiequilibrium is related to the one of the excess electrons through the mass ratio i.e.  $F_{X^-}(T) = F_e\left(T \frac{M_{X^-}^*}{m_e^*}\right)$  [37,44], where  $m_e^*$  and  $M_{X^-}^* = 2m_e^* + m_h^*$  are the electron and trion effective masses,  $m_h^*$  is the hole effective mass (see Figs. S5(a) and (b) [25]). The formation of optically bright trions, which requires extra carriers within the light cone, is favored at low temperatures, resulting in a large trion oscillator strength. The creation of neutral excitons is quenched due to Pauli blocking, as well as by screening due to the presence of free carriers [45]. As temperature increases, trions redistribute towards higher energies and away from the light cone (Fig. 3(b) and Fig. S5(c)-(e) [25]). This process reduces the number of optically active trions, leading to a reduction of their oscillator strength. Simultaneously, the formation of neutral excitons is enhanced due to an increased number of unoccupied states around the K points, leading to an increase of exciton oscillator strength.

We phenomenologically model the oscillator strength of trions  $f_{X^-}$  at different temperatures by a broadened-step F-D-like function (Fig. S5(f) [25]):

$$f_{X^-}(T) = \frac{f_0}{1 + \exp\left(\frac{T - T_0}{T_\gamma}\right)} \quad (1)$$

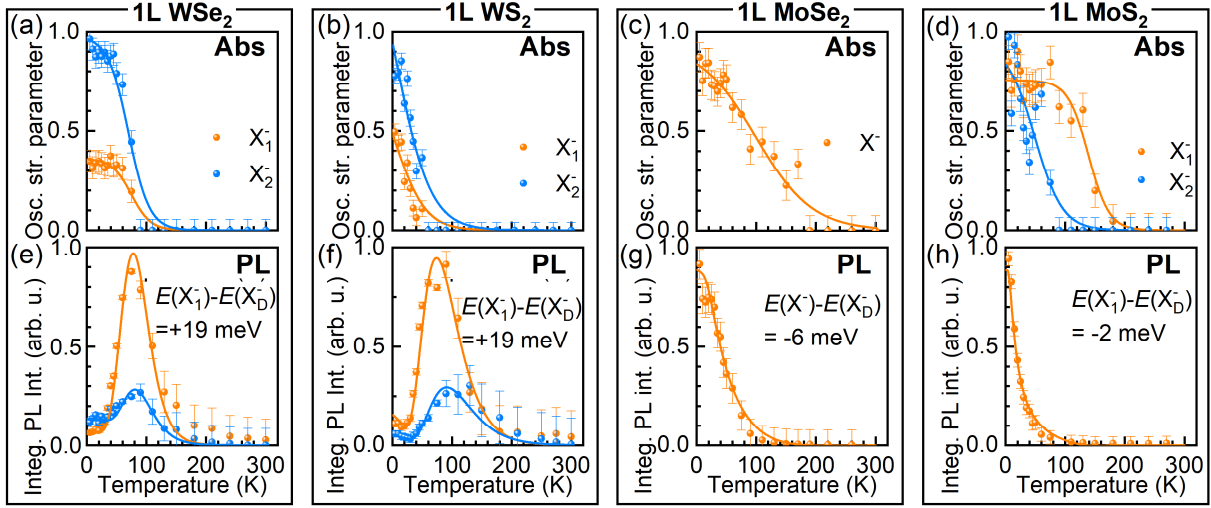


**Figure 2.** Oscillator strength of the trions (orange and blue spheres) deduced from the measured absorption spectra as a function of temperature for hBN-encapsulated (a) WSe<sub>2</sub>, (b) WS<sub>2</sub>, (c) MoSe<sub>2</sub>, and (d) MoS<sub>2</sub> monolayers. Solid lines are the fitted curves using Eq. 1, as explained in the main text. (e) to (h) show the integrated photoluminescence (PL) intensities of the trions obtained from fitting the measured PL spectra as a function of temperature for the four materials. Solid lines are the fitted curves using Eq. 2 as explained in the main text.

where  $f_0$  is the oscillator strength parameter in the limit of  $T = 0$  K, and  $T_\gamma$  is the width of the distribution around the temperature  $T_0$ . The fitted parameters are provided in Table S2 [25]. The exact values of  $T_0$  and  $T_\gamma$  depend on i) the complicated interplay of various trion-scattering processes such as phonon-mediated intravalley scattering, intervalley scattering between  $K^\pm$  valleys or other points of the Brillouin zone, ii) the curvatures of the bands, and iii) the doping density in the different materials. In the next section, we will use these fitted functions of the oscillator strength for calculating the temperature-dependent behavior of PL intensities of the trions.

**Temperature dependence of the trion photoluminescence.** For WSe<sub>2</sub>, the PL intensity of both trions steadily increases up to  $T = 70$  K, followed by a decrease (Fig. 2(e)). For WS<sub>2</sub>, the PL intensity of both trions shows an initial reduction up to  $T = 30$  K, also followed by an increase up to  $T = 70$  K, and a decrease at higher temperatures (Fig. 2(f)). Figures 2(g) and 2(h) depict the measured trion emission intensities of MoSe<sub>2</sub> and MoS<sub>2</sub>. They strongly differ from the W-based materials, because, here, the emission intensity decreases with rising temperature.

The striking behavior of the two W-based materials is explained as follows. In the simplest approximation, the trion PL intensity is proportional to the number density of the optically active trions  $n_{X^-}$  (at thermal equilibrium) around the K points of the Brillouin zone within the light cone and their oscillator strengths  $f_{X^-}(T)$ :

$$I_{X^-}(T) = n_{X^-}(T) f_{X^-}(T) = \left( n_{bg} + \frac{n_0}{1 + \exp\left(\frac{E(X^-) - E(X_D^-)}{k_B T}\right)} \right) f_{X^-}(T). \quad (2)$$

Here,  $n_0$  is the total (bright and dark) number density of trions,  $E(X^-)$  and  $E(X_D^-)$  are the energies of the bright and the dark trion,  $n_{bg} f_{X^-}(T)$  is the PL background, representing a possible PL increase due to optical doping or a PL decrease due to non-radiative processes, and  $k_B$  is the Boltzmann constant. Unlike neutral excitons, an extra electron is required for the creation of negative trions. Therefore, the population of trions in quasithermal equilibrium at low excitation densities is directly proportional to the number density of excess electrons. To recombine and emit a photon, a trion should be located within the light cone to satisfy the linear momentum conservation. In addition, the three carriers constituting a trion need to have the correct spin orientation to be optically bright (Fig. S1 [25]). In steady state, one can assume a F-D distribution of the bright and dark trions. In this case, the trion luminescence from the bright states is governed by F-D statistics. In first approximation, neutral excitons, being bosons, do not directly participate in this process. In W-based materials, the lowest energy trion state is optically dark (Fig. S1(c) [25]) [1,4,6,8–10,14,15,17,46], leading to an inefficient PL emission (Fig. 3(b)) at low temperatures. When the temperature is initially increased ( $5 \text{ K} < T < 30 \text{ K}$ ), the oscillator strength of WS<sub>2</sub> ( $f_{X^-}(T)$  in Eq. 2) drops sharply (Fig. 2(b)), while it decreases only slightly for WSe<sub>2</sub> (Fig. 2(a)). As a consequence, the trion PL intensity of WS<sub>2</sub> falls initially, while it shows a slight increase for WSe<sub>2</sub>. With rising temperature ( $30 \text{ K} < T < 70 \text{ K}$ ), the bright-trion state with energy  $E(X^-)$  is increasingly populated following a F-D distribution, resulting in a stronger PL (Fig. 3(b), right panel) for both materials. However, as the trion oscillator strength  $f_{X^-}$  drastically decreases at higher temperatures  $T > 70 \text{ K}$  (Figs. 2(a) and 2(b)), the PL intensity decreases again for both W-based materials.

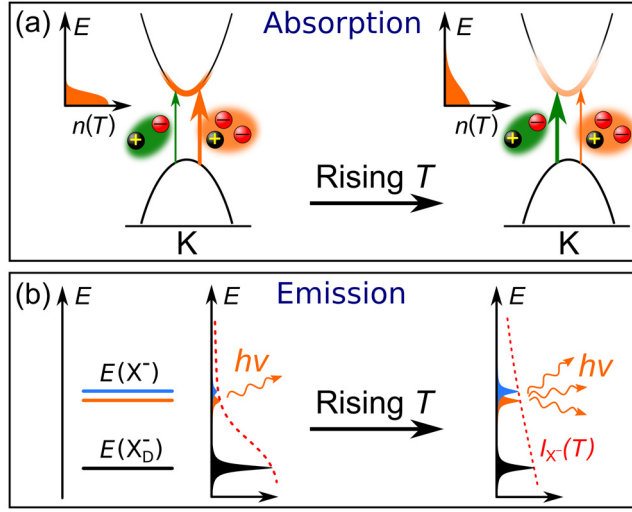


**Figure 3.** (a) Schematic drawing visualizing the transfer of oscillator strength in optical absorption between neutral excitons (green vertical arrow) and trions (orange vertical arrow) with rising temperature, as explained in the main text. A thicker vertical arrow represents a larger transition strength. It reduces for trions with rising temperature. (b) Schematic drawing visualizing the increasing emission intensity of the bright trion when the temperature rises for W-based TMDC monolayers, as explained in the main text.

We use Eq. (2) to fit the trion PL intensities of WSe<sub>2</sub> and WS<sub>2</sub> in Figs. 2(e) and 2(f) (solid lines). The energies of the two bright trions  $E(X_1^-)$  and  $E(X_2^-)$  are fixed to the values obtained from the measured PL spectra, and an additional dark-trion state of energy  $E(X_D^-)$  is assumed. The two trion-intensity curves are collectively fit only using PL data for  $T \leq 150$  K, so that a role of non-radiative processes and phonon-absorption-related processes at higher temperatures is minimized. From our fitting (Table 1), we find that the additional (dark) trion state  $X_D^-$  is located  $19 \pm 3$  meV below the lowest bright trion  $X_1^-$  both in WSe<sub>2</sub> and WS<sub>2</sub> (Fig. 4). This value is in excellent agreement with recent gate-voltage-dependent PL studies in hBN-encapsulated WSe<sub>2</sub>, where the reported numbers are 20 meV [23] and 22 meV [47]. We emphasize that we obtain the same value of  $E(X_D^-)$  within our error bars for both materials, when applying our model to each bright trion independently (unlike fitting the two trions collectively above, where a common  $E(X_D^-)$  was assumed).

**Table 1.** Energies of the dark trion  $X_D^-$ , bright trions ( $X_1^-$  and  $X_2^-$ ) and the bright exciton  $X^0$  in the four materials. The last two columns show the energy difference of  $X_D^-$ , with respect to the  $X_1^-$ , in experiment and *GW-BSE ab-initio* calculations.

Monolayer (hBN encapsulated)	Transition energy (meV)				$E(X_1^-) - E(X_D^-)$ (meV)	
	$X_D^-$ (Exp.)	$X_1^-$ (Exp.)	$X_2^-$ (Exp.)	$X^0$ (Exp.)	Exp.	Th.
WSe <sub>2</sub>	1677±3	1691±1	1697±1	1727±1	+19±3	+30±10
WS <sub>2</sub>	1981±3	1998±1	2004±1	2035±1	+19±3	+30±10
MoSe <sub>2</sub>	1609±3	1603±1	-	1630±1	-6±3	+5±10
MoS <sub>2</sub>	1938±3	1936±1	1943±1	1966±1	-2±3	+10±10

For MoS<sub>2</sub>, only  $X_1^-$  is used in our model, since  $X_2^-$  is very weak in PL and cannot be tracked at higher temperatures. We find a dark-trion state located  $6 \pm 3$  meV and  $2 \pm 3$  meV above the bright-trion state for MoSe<sub>2</sub> and MoS<sub>2</sub>, respectively, elucidating the “optically-bright nature” of Mo-based materials (Fig. 4). Importantly, it is not possible to model the experimental data, if the dark-trion states are neglected in the two bright materials i.e. MoSe<sub>2</sub> and MoS<sub>2</sub>.

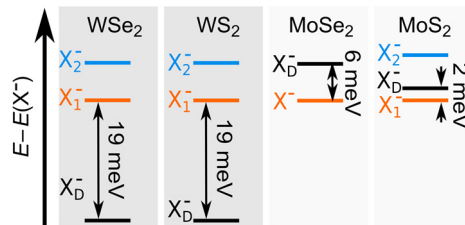


**Figure 4.** Relative energies of dark trion  $X_D^-$  with respect to the bright trion  $X_1^-$ , for hBN-encapsulated monolayers of WSe<sub>2</sub>, WS<sub>2</sub>, MoSe<sub>2</sub> and MoS<sub>2</sub>, derived from the experiment and modeling. The second bright trion  $X_2^-$  is also marked. For MoSe<sub>2</sub>, only one bright trion  $X^-$  is measured and drawn.

**Nature of dark-trion states.** For dark transitions, two mechanisms have to be considered: (a) spin-forbidden transitions, and (b) momentum-indirect transitions [19]. Our experiments point towards spin-forbidden dark excitons. Momentum-dark states can show photoluminescence at rising temperatures because of phonon-assisted recombination processes. Thus a PL line emerges or is enhanced [48,49]. However, we do not observe this behavior in our experiment. Furthermore, transitions from dark to bright trions would need to absorb phonons in case of momentum-dark transitions and thus would distinctly deviate from a Fermi-Dirac distribution, which is contrary to our results.

In conclusion, we observe a strongly different behavior of the photoluminescence emission of trions in WSe<sub>2</sub>, WS<sub>2</sub> vs. MoSe<sub>2</sub>, and MoS<sub>2</sub> monolayers as a function of temperature. Our experimental results are excellently modelled by a dark-trion state energetically below the bright trions in WSe<sub>2</sub> and WS<sub>2</sub>, and by a dark-trion state almost equal in energy with the bright trion in MoSe<sub>2</sub> and MoS<sub>2</sub>. These results are also in good agreement with our *ab-initio* calculations based on *GW*-BSE theory. Our work provides a comprehensive understanding of the radiative phenomena in doped TMDCs as a function of temperature, and is important for a new generation of valleytronic devices involving the creation and readout of long-lived dark trions.

**Acknowledgements.** The authors acknowledge financial support from the German Research Foundation (DFG projects no. AR 1128/1-1, AR 1128/1-2, and DE 2749/2-1). MP and PK were supported by the ATOMOPTO project carried out within the TEAM programme of the Foundation for Polish Science co-financed by the European Union under the European Regional Development Fund. The computing time granted by the Paderborn Center for Parallel Computing (PC2) is gratefully acknowledged.

## REFERENCES.

- [1] A. Arora, K. Nogajewski, M. Molas, M. Koperski, and M. Potemski, *Nanoscale* **7**, 20769 (2015).
- [2] G. Wang, C. Robert, A. Suslu, B. Chen, S. Yang, S. Alamdari, I. C. Gerber, T. Amand, X. Marie, S. Tongay, and B. Urbaszek, *Nat. Commun.* **6**, 10110 (2015).
- [3] J. Jadczyk, J. Kutrowska-Girzycka, P. Kapuściński, Y. S. Huang, A. Wójs, L. Bryja, J. Kutrowska-Girzycka, P. Kapuscinski, Y. S. Huang, A. Wojs, and L. Bryja, *Nanotechnology* **28**, 395702 (2017).
- [4] X.-X. Zhang, Y. You, S. Y. F. Zhao, and T. F. Heinz, *Phys. Rev. Lett.* **115**, 257403 (2015).
- [5] I. G. Lezama, A. Arora, A. Ubaldini, C. Barreateau, E. Giannini, M. Potemski, and A. F. Morpurgo, *Nano Lett.* **15**, 2336 (2015).
- [6] A. Arora, M. Koperski, K. Nogajewski, J. Marcus, C. Faugeras, and M. Potemski, *Nanoscale* **7**, 10421 (2015).
- [7] M. R. Molas, K. Nogajewski, A. O. Slobodeniuk, J. Binder, M. Bartos, and M. Potemski, *Nanoscale* **9**, 13128 (2017).
- [8] G.-B. Liu, W.-Y. Shan, Y. Yao, W. Yao, and D. Xiao, *Phys. Rev. B* **88**, 085433 (2013).
- [9] M. Koperski, M. R. Molas, A. Arora, K. Nogajewski, A. O. Slobodeniuk, C. Faugeras, and M. Potemski, *Nanophotonics* **6**, 1289 (2017).
- [10] G. Wang, C. Robert, M. M. Glazov, F. Cadiz, E. Courtade, T. Amand, D. Lagarde, T. Taniguchi, K. Watanabe, B. Urbaszek, and X. Marie, *Phys. Rev. Lett.* **119**, 047401 (2017).
- [11] J. Quereda, T. S. Ghiasi, F. A. van Zwol, C. H. van der Wal, and B. J. van Wees, *2D Mater.* **5**, 015004 (2017).
- [12] C. Robert, T. Amand, F. Cadiz, D. Lagarde, E. Courtade, M. Manca, T. Taniguchi, K. Watanabe, B. Urbaszek, and X. Marie, *Phys. Rev. B* **96**, 155423 (2017).
- [13] K. P. Loh, *Nat. Nanotechnol.* **12**, 837 (2017).
- [14] T. Deilmann and K. S. Thygesen, *Phys. Rev. B* **96**, 201113 (2017).
- [15] M. R. Molas, C. Faugeras, A. O. Slobodeniuk, K. Nogajewski, M. Bartos, D. M. Basko, and M. Potemski, *2D Mater.* **4**, 021003 (2017).
- [16] Y. Zhou, G. Scuri, D. S. Wild, A. A. High, A. Dibos, L. A. Jauregui, C. Shu, K. De Greve, K. Pistunova, A. Y. Joe, T. Taniguchi, K. Watanabe, P. Kim, M. D. Lukin, and H. Park, *Nat. Nanotechnol.* **12**, 856 (2017).
- [17] X.-X. Zhang, T. Cao, Z. Lu, Y.-C. Lin, F. Zhang, Y. Wang, Z. Li, J. C. Hone, J. A. Robinson, D. Smirnov, S. G. Louie, and T. F. Heinz, *Nat. Nanotechnol.* **12**, 883 (2017).
- [18] M. Selig, G. Berghäuser, M. Richter, R. Bratschitsch, A. Knorr, and E. Malic, *2D Mater.* **5**, 035017 (2018).
- [19] T. Mueller and E. Malic, *Npj 2D Mater. Appl.* **2**, 29 (2018).
- [20] K. F. Mak, K. He, C. Lee, G. H. Lee, J. Hone, T. F. Heinz, and J. Shan, *Nat. Mater.* **12**, 207 (2013).
- [21] G. Wang, A. Chernikov, M. M. Glazov, T. F. Heinz, X. Marie, T. Amand, and B. Urbaszek, *Rev. Mod. Phys.* **90**, 021001 (2018).
- [22] G. Plechinger, P. Nagler, A. Arora, R. Schmidt, A. Chernikov, A. G. A. G. del Águila, P. C. M. P. C. M. Christianen, R. Bratschitsch, C. Schüller, and T. Korn, *Nat. Commun.* **7**, 12715 (2016).
- [23] E. Liu, J. van Baren, Z. Lu, M. M. Altaïary, T. Taniguchi, K. Watanabe, D. Smirnov, and C. H. Lui, *Phys. Rev. Lett.* **123**, 027401 (2019).
- [24] J. R. Schaibley, H. Yu, G. Clark, P. Rivera, J. S. Ross, K. L. Seyler, W. Yao, and X. Xu, *Nat. Rev. Mater.* **1**, 16055 (2016).
- [25] *Supplemental Material* (6 supporting figures, details on theoretical results, sample preparation, experimental setup, absorption and photoluminescence spectra at all temperatures, transfer of oscillator strength between trions and

excitons, and its pictorial explanation).

- [26] M. Rohlfing and S. G. Louie, *Phys. Rev. B* **62**, 4927 (2000).
- [27] G. Onida, L. Reining, and A. Rubio, *Rev. Mod. Phys.* **74**, 601 (2002).
- [28] T. Deilmann, M. Drüppel, and M. Rohlfing, *Phys. Rev. Lett.* **116**, 196804 (2016).
- [29] T. Deilmann and K. S. Thygesen, *2D Mater.* **6**, 035003 (2019).
- [30] D. Van Tuan, B. Scharf, Z. Wang, J. Shan, K. F. Mak, I. Žutić, and H. Dery, *Phys. Rev. B* **99**, 085301 (2019).
- [31] F. Cadiz, E. Courtade, C. Robert, G. Wang, Y. Shen, H. Cai, T. Taniguchi, K. Watanabe, H. Carrere, D. Lagarde, M. Manca, T. Amand, P. Renucci, S. Tongay, X. Marie, and B. Urbaszek, *Phys. Rev. X* **7**, 021026 (2017).
- [32] O. A. Ajayi, J. V Ardelean, G. D. Shepard, J. Wang, A. Antony, T. Taniguchi, K. Watanabe, T. F. Heinz, S. Strauf, X.-Y. Zhu, and J. C. Hone, *2D Mater.* **4**, 031011 (2017).
- [33] J. Wierzbowski, J. Klein, F. Sigger, C. Straubinger, M. Kremser, T. Taniguchi, K. Watanabe, U. Wurstbauer, A. W. Holleitner, M. Kaniber, K. Müller, and J. J. Finley, *Sci. Rep.* **7**, 12383 (2017).
- [34] G. Wang, L. Bouet, D. Lagarde, M. Vidal, A. Balocchi, T. Amand, X. Marie, and B. Urbaszek, *Phys. Rev. B* **90**, 075413 (2014).
- [35] Z. Li, T. Wang, C. Jin, Z. Lu, Z. Lian, Y. Meng, M. Blei, S. Gao, T. Taniguchi, K. Watanabe, T. Ren, S. Tongay, L. Yang, D. Smirnov, T. Cao, and S.-F. Shi, *Nat. Commun.* **10**, 2469 (2019).
- [36] J. G. Roch, G. Froehlicher, N. Leisgang, P. Makk, K. Watanabe, T. Taniguchi, and R. J. Warburton, *Nat. Nanotechnol.* **14**, 432 (2019).
- [37] V. Ciulin, P. Kossacki, S. Haacke, J.-D. Ganière, B. Deveaud, A. Esser, M. Kutrowski, and T. Wojtowicz, *Phys. Rev. B* **62**, R16310 (2000).
- [38] G. V Astakhov, V. P. Kochereshko, D. R. Yakovlev, W. Ossau, J. Nürnberger, W. Faschinger, and G. Landwehr, *Phys. Rev. B* **62**, 10345 (2000).
- [39] P. Kossacki, *J. Phys. Condens. Matter* **15**, R471 (2003).
- [40] A. Arora, T. Deilmann, T. Reichenauer, J. Kern, S. Michaelis de Vasconcellos, M. Rohlfing, and R. Bratschitsch, *Phys. Rev. Lett.* **123**, 167401 (2019).
- [41] H. Buhmann, L. Mansouri, J. Wang, P. H. Beton, N. Mori, L. Eaves, M. Henini, and M. Potemski, *Phys. Rev. B* **51**, 7969 (1995).
- [42] G. V. Astakhov, V. P. Kochereshko, D. R. Yakovlev, W. Ossau, J. Nürnberger, W. Faschinger, G. Landwehr, T. Wojtowicz, G. Karczewski, and J. Kossut, *Phys. Rev. B* **65**, 115310 (2002).
- [43] M. Koperski, M. R. Molas, A. Arora, K. Nogajewski, M. Bartos, J. Wyzula, D. Vaclavkova, P. Kossacki, and M. Potemski, *2D Mater.* **6**, 015001 (2018).
- [44] A. Esser, E. Runge, R. Zimmermann, and W. Langbein, *Phys. Rev. B* **62**, 8232 (2000).
- [45] P. Płochocka, P. Kossacki, W. Maślana, J. Cibert, S. Tatarenko, C. Radzewicz, and J. A. Gaj, *Phys. Rev. Lett.* **92**, 177402 (2004).
- [46] J. P. Echeverry, B. Urbaszek, T. Amand, X. Marie, and I. C. Gerber, *Phys. Rev. B* **93**, 121107 (2016).
- [47] Z. Li, T. Wang, Z. Lu, M. Khatoniari, Z. Lian, Y. Meng, M. Blei, T. Taniguchi, K. Watanabe, S. A. McGill, S. Tongay, V. M. Menon, D. Smirnov, and S.-F. Shi, *Nano Lett.* **19**, 6886 (2019).
- [48] J. Kunstmann, F. Mooshammer, P. Nagler, A. Chaves, F. Stein, N. Paradiso, G. Plechinger, C. Strunk, C. Schüller, G. Seifert, D. R. Reichman, and T. Korn, *Nat. Phys.* **14**, 801 (2018).
- [49] T. V. Shubina, M. Remškar, V. Y. Davydov, K. G. Belyaev, A. A. Toropov, and B. Gil, *Ann. Phys.* **531**, 1800415 (2019).



## Supplemental Material

**Samples and experiment.** Monolayers of the transition metal dichalcogenide (TMDC) semiconductors WSe<sub>2</sub>, WS<sub>2</sub>, MoSe<sub>2</sub>, and MoS<sub>2</sub> are mechanically exfoliated from the corresponding bulk single crystals (HQ Graphene, Groningen, The Netherlands) using the scotch tape method. Thin flakes (few tens of nm thickness) of hBN are mechanically exfoliated from bulk single crystals (HQ Graphene, Groningen, The Netherlands) with scotch tape as well. A hBN flake, a TMDC monolayer and another hBN flake are successively transferred on a 500  $\mu\text{m}$  thick sapphire substrate using a dry transfer method [S1]. Each dry transfer step is followed by annealing at a temperature of 200°C under ambient conditions for 15 minutes. This method ensures good interfacial quality between hBN layers and the TMDC monolayers, which reduces the exciton linewidths, approaching the homogeneous regime.

Optical spectroscopy is performed by keeping the samples in an optical continuous flow He cryostat. For retrieving an absorption spectrum  $A(\lambda)$ , reflectivity  $R(\lambda)$  and transmission  $T(\lambda)$  spectra are measured on the same location of the sample under the same experimental conditions. The optical absorption of the sample is calculated as  $A(\lambda) = 1 - R(\lambda) - T(\lambda)$ . For the reflectivity measurement, light from either a broadband LED source (for WS<sub>2</sub> and MoS<sub>2</sub>) or a tungsten halogen lamp (for WSe<sub>2</sub> and MoSe<sub>2</sub>) is incident on the sample through a 50x long working distance objective lens (numerical aperture NA = 0.55). The reflected light is dispersed using a monochromator with 300 mm focal length, and the spectrum is measured with a peltier-cooled charge coupled device camera. The system response (reference spectrum) is measured by reflecting light from the bare sapphire substrate area close to the hBN/TMDC/hBN structure. Transmission spectra are taken in a similar manner, except that the light is incident on the sample via a achromatic doublet convex lens with 75 mm focal length. For photoluminescence (PL) measurements, a continuous wave laser of 532 nm (2.22 eV) wavelength is focused on a diffraction limited spot. The focused power is noted on the y axis of Figs. 1(e-h) in the main text for the four TMDC materials. Low-temperature spectra ( $T = 5\text{K}$ ) for the four samples are presented in Fig. S2.

**Absorption and photoluminescence line widths.** The line widths of the trion and exciton resonances lie between 1.8 meV and 6.8 meV (Table S1), which demonstrates the excellent quality of the samples. Unresolved resonances are marked with a hyphen. For the transition energies of the resonances, we refer to Table 1 of the main text.

**Table S1.** Low-temperature ( $T = 5\text{K}$ ) FWHM line widths of excitons (X) and trions ( $X_1^-$ ,  $X_2^-$ ) derived from PL and absorption spectra of the four TMDC monolayer crystals encapsulated in hBN

Material (encapsulated with hBN)	Full-width at half-maximum line width (meV)					
	$X_1^-$		$X_2^-$		$X^0$	
	Abs.	PL	Abs.	PL	Abs.	PL
1L WSe <sub>2</sub>	4.0	3.2	5.0	4.8	4.4	6.8
1L WS <sub>2</sub>	2.0	2.6	2.6	2.1	5.5	6.6
1L MoSe <sub>2</sub>	4.0	5.4	—	—	4.0	6.7
1L MoS <sub>2</sub>	2.3	1.8	4.4	—	4.0	2.4

**Table S2.**  $T_0$  and  $T_\gamma$  parameters obtained after fitting Eq. (1) to data in Figs. 2(a) to 2(d).

Material (encapsulated with hBN)	$T_0$ (K)		$T_\gamma$ (K)	
	$X_1^-$	$X_2^-$	$X_1^-$	$X_2^-$
1L WSe <sub>2</sub>	70	75	16	17
1L WS <sub>2</sub>	5	5	25	30
1L MoSe <sub>2</sub>	100	—	46	—
1L MoS <sub>2</sub>	140	50	17	23

## REFERENCES.

- [S1] A. Castellanos-Gomez, M. Buscema, R. Molenaar, V. Singh, L. Janssen, H. S. J. van der Zant, and G. a Steele, 2D Mater. **1**, 011002 (2014).
- [S2] T. Deilmann and K. S. Thygesen, Phys. Rev. B **96**, 201113 (2017).
- [S3] M. Dr ppel, T. Deilmann, P. Kr ger, and M. Rohl ng, Nat. Commun. **8**, 2117 (2017).

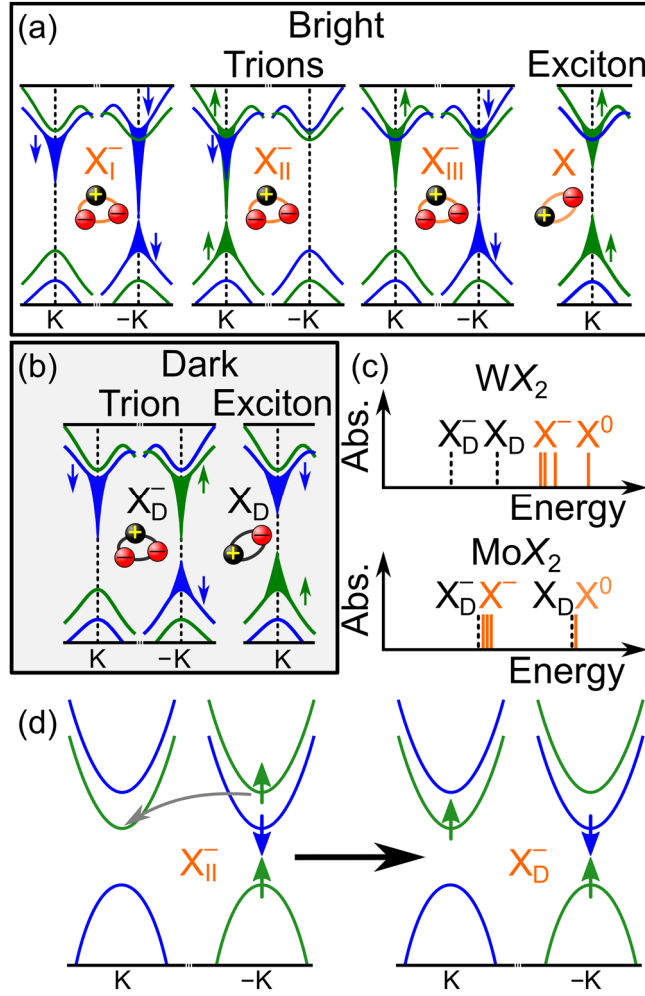


**Figure S1.** (a) k-space representation of the three possible types of bright trions,  $X_I^-$ ,  $X_{II}^-$  and  $X_{III}^-$  (not to be confused with labels of experimentally observed trions  $X_1^-$  and  $X_2^-$  in the main text) and the bright exciton  $X^0$  in the monolayers of W-based semiconducting transition metal dichalcogenides where bands are colored blue (down spin) and green (up spin). The bands participating in the creation of an excitation are represented by elongated filled cones. The third trion ( $X_{III}^-$ ) has both electrons in the upper conduction bands, and is expected to have low oscillator strength, explaining its absence in the experiments. (b) is similar to (a) for the dark excitations (see Ref. [S2] for details). Excitations similar to those shown in (a) and (b) with opposite spin and valley character are also possible but not displayed for brevity. (c) Schematic drawing showing the relative energetic positions of the dark excitations (black dashed) with respect to the bright (orange) absorption lines in W- and Mo-based TMDC monolayers. For W-based materials, dark states  $X_D$  and  $X_D^-$  are lower in energy than the bright states  $X^0$  and  $X_D$ , in contrast to Mo-based materials, where the dark exciton (trion) is in close proximity to the bright exciton (trion). In the presence of hBN layers encapsulating the TMDC monolayer, a large band gap renormalization and a small red-shift of the excitations occurs [S3]. However, the effect of surrounding hBN on the relative separation between bright and dark trions (when compared to vacuum around the monolayer) is less than 10 meV, which is within our numerical accuracy (d) Bright trions can convert to dark trions and vice versa via intervalley scattering processes of the excess carriers, without the requirement of a spin flip. An example of one such process is shown.



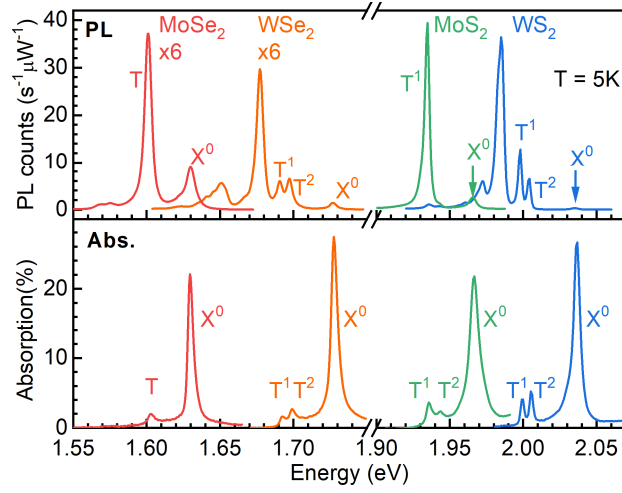


**Figure S2. Low-temperature excitonic spectra.** (Top) Low-temperature ( $T = 5\text{K}$ ) photoluminescence spectra MoSe<sub>2</sub>, WSe<sub>2</sub>, MoS<sub>2</sub>, and WS<sub>2</sub> monolayers encapsulated in hBN. A 532 nm CW laser with diffraction-limited focus on the sample and a focused power of 500  $\mu\text{W}$ , 200  $\mu\text{W}$ , 60  $\mu\text{W}$ , and 80  $\mu\text{W}$ , respectively is used for the PL measurements. PL counts are divided by the accumulation time as well as power (in  $\mu\text{W}$ ) to directly compare the four cases. MoSe<sub>2</sub> and WSe<sub>2</sub> spectra are amplified by factors of 6 for clarity. (bottom) Corresponding measured absorption spectra  $A(\lambda) = 1 - R(\lambda) - T(\lambda)$  for the four samples.

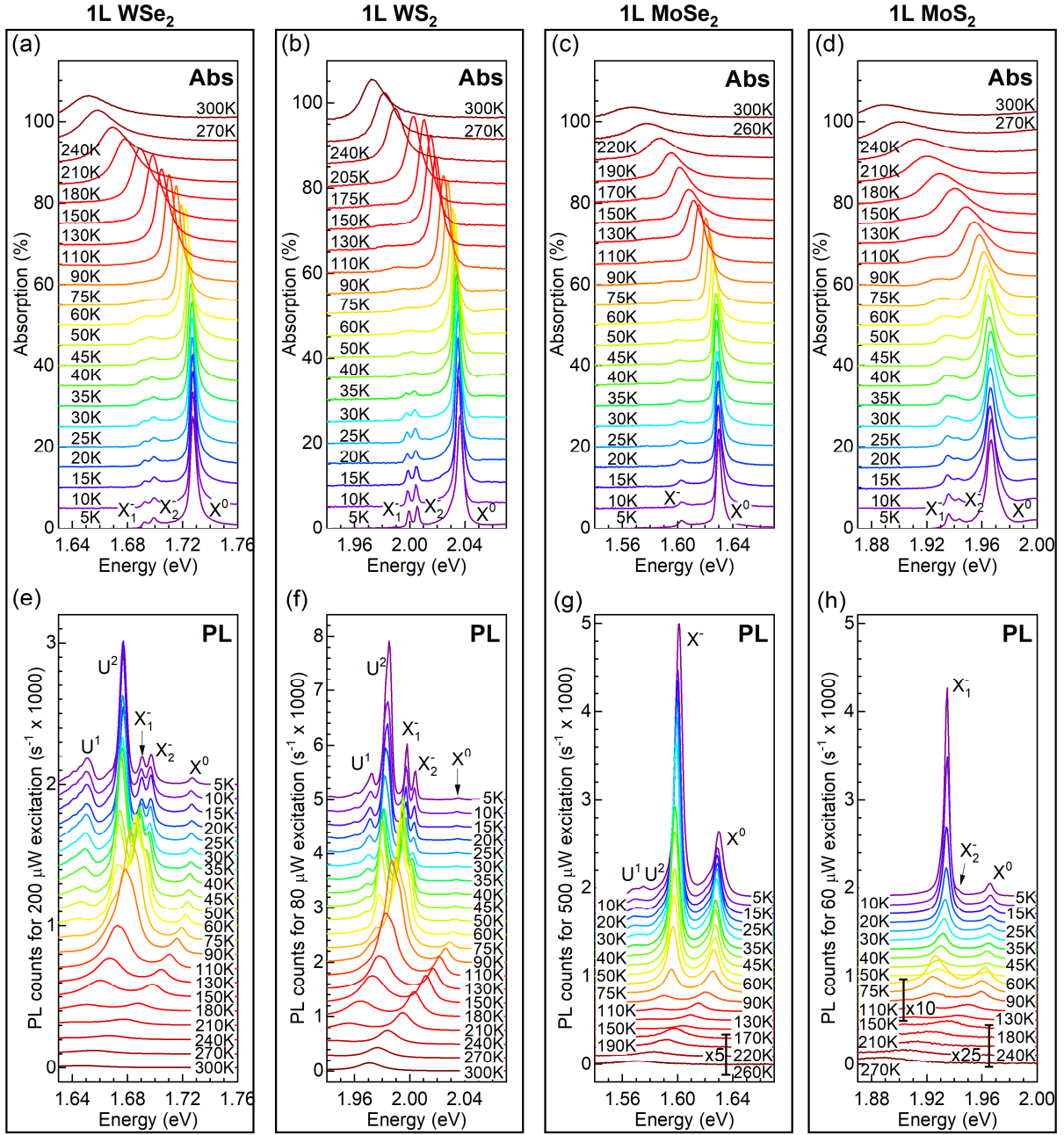


**Figure S3. Absorption and PL spectra for all temperatures.** Optical absorption spectra of hBN-encapsulated (a) WSe<sub>2</sub>, (b) WS<sub>2</sub>, (c) MoSe<sub>2</sub>, and (d) MoS<sub>2</sub> monolayers on sapphire substrate, as a function of temperature  $T = 5 - 300$  K. (e) to (h) photoluminescence spectra of the four materials as a function of temperature. The spectra are vertically shifted for clarity. Low PL intensities in (g) and (h) are amplified by factors mentioned with the spectra.

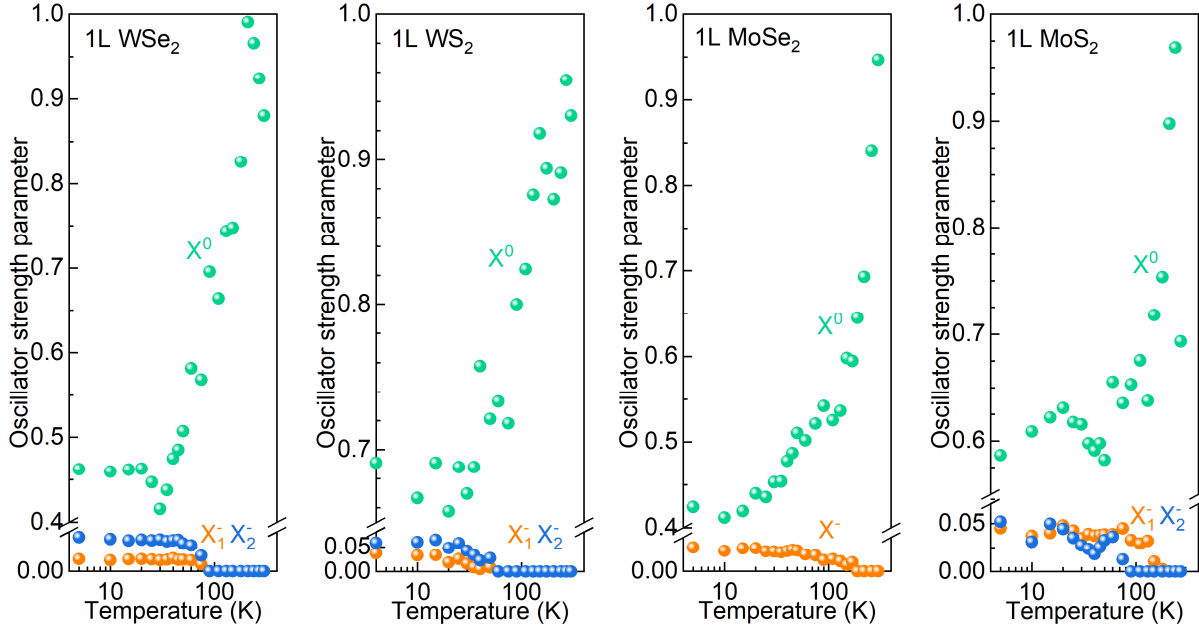


**Figure S4. Oscillator strength transfer between excitons and trions.** Temperature-dependent oscillator strength parameters derived from the line shape analysis of the absorption spectra of monolayers of WSe<sub>2</sub>, WS<sub>2</sub>, MoSe<sub>2</sub>, and MoS<sub>2</sub> encapsulated in hBN are plotted. For all four TMDC monolayers, the oscillator strength of the neutral exciton rises, while that of charged excitons reduces. A Fermi-Dirac distribution based model explains the observed trend as discussed in the main text.

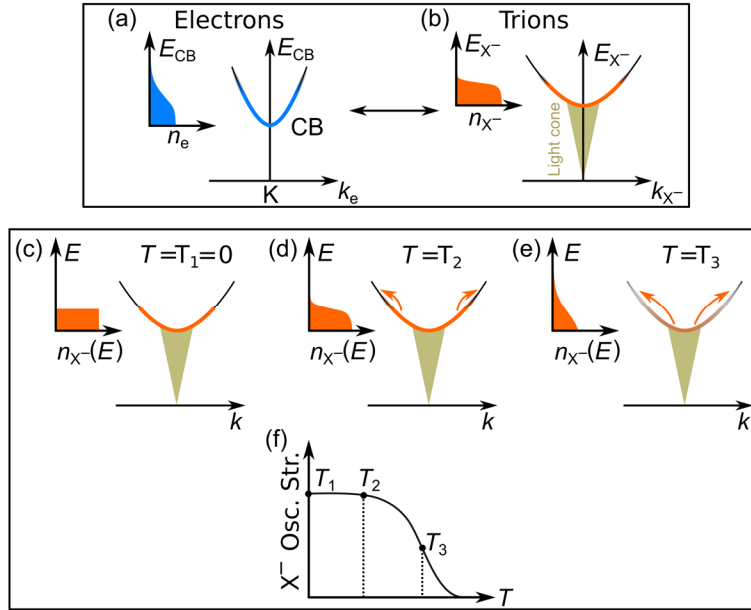


**Figure S5. Change of trion oscillator strength with temperature.** a) Thermal distribution of electrons in the conduction band (CB), and (b) of trions (having a smaller curvature or larger mass than CB), in momentum space. The F-D distribution functions in the two cases are related by  $F_{X^-}(T) = F_e(T m_{X^-}^*/m_e^*)$ , i.e. the temperature is rescaled by the mass ratio of the quasiparticles. (c) At  $T = T_1 = 0$ , the trions occupy the states close to the minimum. Trions within the light cone are optically active, resulting in a large oscillator strength, as shown in (f). (d) For  $T = T_2 > T_1$ , trions outside the light cone redistribute to higher energies. However, the population within the light cone is largely unaffected, and the oscillator strength is similar to that in (c). (e) For even higher temperature ( $T = T_3$ ), the trion population within the light cone spills out to higher energies, and the oscillator strength is substantially reduced, as depicted in (f).

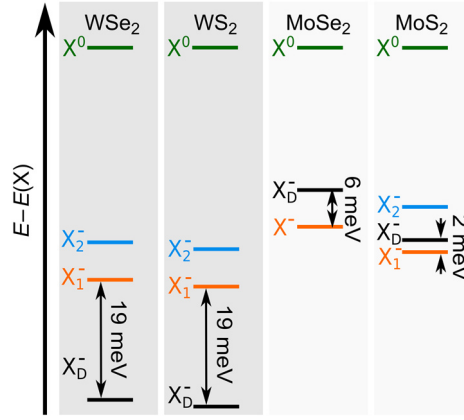


**Figure S6. Energetic positions of trions relative to neutral excitons.** Relative energies of the bright trions ( $X_1^-$  and  $X_2^-$ ) and the dark trion  $X_D^-$  with respect to the neutral exciton  $X^0$  for hBN-encapsulated monolayers of WSe<sub>2</sub>, WS<sub>2</sub>, MoSe<sub>2</sub> and MoS<sub>2</sub>, derived from the experiment and modeling. For MoSe<sub>2</sub>, only one bright trion  $X^-$  is measured and drawn.